Wavelet Based Restoration of Images with Missing or Damaged Pixels

Hui Ji[*,1], Zuowei Shen[1] and Yuhong Xu[2]

[1] *Department of Mathematics, National University of Singapore, 2 Science Drive 2, Singapore 117543.*
[2] *Temasek Laboratories, National University of Singapore, 2 Science Drive 2, Singapore 117543.*

Abstract. This paper addresses the problem of how to restore degraded images where the pixels have been partly lost during transmission or damaged by impulsive noise. A wide range of image restoration tasks is covered in the mathematical model considered in this paper – *e*.g. image deblurring, image inpainting and super-resolution imaging. Based on the assumption that natural images are likely to have a sparse representation in a wavelet tight frame domain, we propose a regularization-based approach to recover degraded images, by enforcing the analysis-based sparsity prior of images in a tight frame domain. The resulting minimization problem can be solved efficiently by the split Bregman method. Numerical experiments on various image restoration tasks – simultaneously image deblurring and inpainting, super-resolution imaging and image deblurring under impulsive noise – demonstrated the effectiveness of our proposed algorithm. It proved robust to mis-detection errors of missing or damaged pixels, and compared favorably to existing algorithms.

Key words: Image restoration, impulsive noise, tight frame, sparse approximation, split Bregman method.

1. Introduction

A digital image may be distorted or degraded during image formation or transmission, which can extend to an unacceptable loss of visual image quality. How to recover degraded images has long been a fundamental problem in image processing. There exist many types of image degradations in practice – *e*.g. image blurring by out-of-focusing or camera shake during image acquisition, image/film deterioration due to dust spots or cracks in film, low resolution of images due to physical limits of digital cameras, and noisy images caused by

---

*Corresponding author. *Email addresses:* `matjh@nus.edu.sg` (H. Ji), `matzuows@nus.edu.sg` (Z. Shen), `tslxyh@nus.edu.sg` (Y. Xu)

noisy sensors or transmission errors. For simplicity, if we denote images as vectors in $\mathbb{R}^n$ by concatenating their columns, the observed degraded version of the latent image u can usually be modeled as

$$f = Hu + \epsilon, \tag{1.1}$$

where f is the observed degraded image, u is the latent image, ϵ is the image noise and the matrix H denotes the degrading operator. The image restoration task is then to reverse the effect of the operator H on f to recover the latent image u. It is well known that image restoration is an ill-conditioned inverse problem sensitive to image noise. It makes things even harder when the complete version of the degraded image f is unavailable. This can happen when, for example, some image pixels go missing during the transmission, or some image regions are damaged due to scratches in films. In all these cases, only a subset of image pixels is available or reliable. If Λ denotes the index set of all available image pixels, then the image degradation model (1.1) becomes

$$P_\Lambda f = P_\Lambda(Hu + \epsilon) \tag{1.2}$$

where P_Λ is the projection operator, defined by a diagonal matrix with diagonal entries 1 for the indices in Λ and 0 otherwise.

The goal of this paper is to develop a robust algorithm to solve (1.2) – i.e. to restore the latent image u from its incomplete, degraded and noisy version $P_\Lambda f$. The quite generic operator H in (1.2) includes many types of image degradations. For example, H may be the matrix form of the discrete convolution operator for image deblurring, a projection matrix for image inpainting, or an identity matrix for image denoising. Image restoration with missing or damaged pixels is not only ill-conditioned but also ill-posed with an infinite number of solutions. To recover the latent image u, we need to assume that there exists some structure prior or image redundancy such that all pixels can be inferred from partial degraded information for u. There have been many image priors proposed in the past – *e.g.* the Tikhonov functional-based smoothness prior for images [41], total variation functional [20, 38] or Mumford-Shah functional-based piece-wise smoothness prior [33] for cartoon images, and the exemplar-based local patch redundancy prior of natural images [23]. In recent years, sparsity-based priors of images in certain domains have been used widely in many image restoration tasks, based on the observation that images usually have sparse representations (or sparse approximations) in some transformed domains. For example, there can be Fourier or windowed Fourier transforms, local cosine transforms, wavelet or framelet transforms, or discrete gradient operators. In particular, the sparsity prior of images in tight frame systems [24, 37] has been used successfully in many image restoration tasks, such as image inpainting [11, 12, 16], non-blind image deblurring [15, 16] and blind motion deblurring [13, 14]. All of this sparsity-based research motivates us to investigate the application of the sparsity prior of images in a tight frame domain to solve (1.2), for image restoration with missing or damaged pixels.

In order do so, one may find a sparse solution of (1.2) in the tight frame domain, which can be approximated by solving an ℓ_1-norm regularized minimization problem. Based on different regularization strategies, there are three types of sparsity priors – viz. synthesis-based sparsity prior [15], balanced sparsity prior [12], and analysis-based sparsity prior

[16]. The approach proposed in this paper uses the analysis-based sparsity prior, as it is empirically observed in many imaging applications that this tends to yield the result with less undesirable artifacts. Let $W \in \mathbb{R}^{m \times n}$ be a linear transform, called an analysis operator, acting from $\mathbb{R}^n$ to $\mathbb{R}^m$. The matrix W can be generated by any tight frame transform, and we use redundant transforms in the implementation of the algorithm such that $m \geq n$. Then the resulting minimization from the analysis-based sparsity prior in a tight frame domain is

$$\min_{u} \quad \frac{1}{p}\|P_\Lambda(Hu - f)\|_p^p + \lambda\|Wu\|_1, \tag{1.3}$$

where $\| \cdot \|_p$ denotes the ℓ_p-norm with $p \geq 1$, u is the resulting latent image, f is the degraded image, H is the degradation operator, P_Λ is the projection matrix, W is the tight frame transform and λ is the regularization parameter.

There are a few research publications using a sparsity prior in a tight frame domain to restore images degraded by individual types of image degradations. The balanced sparsity prior in a tight frame domain has been used to solve the problem of image inpainting [12] with $H = I$ being an identity matrix, and the problem of image super-resolution [18] with P_Λ being a sub-sampling operator and H a convolution operator with a particular low-pass filter. In [15], the synthesis-based sparsity prior is proposed to deblur images with full pixels, where H is a convolution operator and Λ is the full image domain. In [16], the analysis-based sparsity prior is used either to deblur images with full pixels or to inpaint images with missing pixels. In comparison, the mathematical formulation and the corresponding numerical algorithm discussed in this paper work for any linear operator H and any projection matrix P_Λ, providing a unified approach to address a wide range of image restoration problems – including image inpainting, image deblurring, super-resolution, removing impulsive noise, or some combination of them. Moreover, the general ℓ_p-norm is used in the fidelity term of the proposed minimization formulation (1.3), instead of the ℓ_2-norm in these existing methods, which could benefit many image restoration tasks in the presence of outliers. As a demonstration, the ℓ_1-norm is used as the fidelity term in the application of removing impulsive noise from images, which leads to better performance compared to the usual ℓ_2-norm based data fidelity.

Compared to the synthesis-based sparsity prior and balanced sparsity prior approaches, the minimization (1.3) using an analysis-based sparsity prior is more challenging to solve, as the ℓ_1 terms involved in (1.3) are non-smooth and non-separable. Recently, a so-called *split Bregman iteration* [28] has been developed to solve this type of ℓ_1-norm related minimization problem, and demonstrated excellent performance and efficiency in many applications in imaging science [16, 27, 27]. In this paper, we propose a modified version of the split Bregman iteration as the numerical solver to (1.3).

The rest of this paper is organized as follows. Section 2 is devoted to the formulation and discussion of (1.3) to image restoration with missing pixels and the detailed numerical solver for (1.3). Three representative image restoration applications related to (1.3) and their numerical experiments are presented in Section 3 – viz.

1. simultaneous image deblurring and inpainting,

2. super-resolution image reconstruction,

3. image deblurring under impulsive noise.

Finally, in Section 4 we briefly summarize the paper and mention possible future work.

2. Tight Frame Based Restoration of Image with Missing Pixels

In this section, we present our formulation and algorithm for image restoration in the presence of missing or damaged pixels. The redundant tight frame system used in our algorithm is the wavelet tight frame without down-sampling in a two variable setting. The piece-wise linear B-spline framelet system [24, 37] is chosen as the wavelet tight frame in our method, due to its implementation simplicity. If we denote the image as a column vector $f \in \mathbb{R}^n$ by concatenating all columns of the image, then the framelet decomposition operator W can be represented by an $m \times n$ matrix with $m > n$ such that the canonical framelet coefficient vector v is defined as $v = Wu$. Once we have the framelet decomposition operator W, the inverse operator or the reconstruction operator is simply W^T – i.e. $u = W^T v$. We emphasize that W is a rectangular matrix with the row dimension m much larger than its column dimension n. Thus, $W^T W = I$ but $WW^T \neq I$. If $WW^T = I$, it becomes an orthonormal wavelet transform without redundancy. Here we remark that W is basically used for notational convenience. In the practical computation, we neither store the matrix nor use matrix multiplications. Instead, there exist efficient algorithms for both framelet decomposition and reconstruction by passing the images/coefficients through a series of discrete framelet filters with a small memory footprint – cf. [17, 25] for more implementation details.

2.1. Minimization Formulation

In the image degradation model (1.2), the availability of the index set Λ of remained image pixels varies with different image restoration tasks. Temporarily, we assume that Λ is given in advance. To seek the solution u from (1.2), we propose to solve the following minimization problem:

$$\min_u \ \frac{1}{p}\|P_\Lambda(Hu - f)\|_p^p + \lambda\|Wu\|_1, \tag{2.1}$$

where the matrix W is the decomposition operator associated with the linear B-spline framelet system. The motivation for the proposed minimization formulation is as follows.

There are two components in the minimization (2.1). The first is the fidelity term and the second is the regularization term. The ℓ_2-norm with $p = 2$ has been used as the distance function in most existing image restoration methods. As the ℓ_2-norm based distance function is known to be sensitive to outliers, the missing or damaged pixels have to be detected in a pre-process with high accuracy in order to achieve high performance. The accurate detection of missing pixels is possible for some applications such as super-resolution imaging, but is very challenging for some other applications such as image deblurring in the presence of impulsive noise. In such a case, the ℓ_1-norm based distance function is

more suitable as it is known to be robust to outliers – [35]. Thus, both ℓ_2-norm and ℓ_1-norm based distance functions are discussed in this paper, and the choice is application dependent (cf. Section 3 for more details).

The regularization term in (2.1) enforces the sparsity of the canonical tight frame coefficients of the solution, as the corresponding canonical coefficient vector is sparse (i.e. a large number of canonical coefficients are equal to close to zero) for a large class of functions (including piece-wise smooth functions). Moreover, it is known that the weighted norm of the canonical frame coefficient vector of a function is equivalent to its function norm in some spaces – *e.g.* Sobolev or Besov spaces (see [5,29] for more details). In particular, it is shown in [5] that the ℓ_1-norm of the canonical tight frame coefficient vector of a function – i.e. the regularization term in (2.1) – is equivalent to its Besov norm under some mild conditions on the underlying tight frame system. Therefore, the regularization term $\|Wu\|_1$ also controls the smoothness of the solution, which is desirable in image restoration as the result tends to have less artifacts. Meanwhile, the sharp edges in the images are still preserved, as the annihilation of small coefficients in the wavelet tight frame domain by ℓ_1-norm minimization tends to sharpen image edges.

The minimization (2.1) is actually one extreme case of a more general sparsity-based minimization formulation discussed in [40] – viz.

$$\min_v \ \ \frac{1}{2}\|GW^T v - g\|_2^2 + \frac{\beta}{2}\|(I - WW^T)v\|_2^2 + \lambda\|v\|_1, \tag{2.2}$$

where G is some matrix and $\beta \geq 0$ is a positive parameter, and v is the frame coefficient vector such that the solution $u = W^T v$. If we set $\beta = \infty$, essentially the middle term in (2.2) enforces the equality constraint:

$$(I - WW^T)v = 0, \quad \text{or equivalently} \quad v \in \text{range}(W).$$

Thus (2.2) is equivalent to

$$\min_u \ \ \frac{1}{2}\|Gu - g\|_2^2 + \lambda\|Wu\|_1. \tag{2.3}$$

Obviously, our formulation (2.1) is the same as the formulation (2.3) above with

$$p := 2, \quad g := P_\Lambda f \quad \text{and} \quad G := P_\Lambda H.$$

Such a minimization formulation is an analysis-based approach, as it enforces the sparsity of the canonical frame coefficients (or analysis coefficients) of the solution. If $\beta = 0$, the second term vanishes and the minimization (2.2) becomes

$$\min_v \ \ \frac{1}{2}\|GW^T v - g\|_2^2 + \lambda\|v\|_1. \tag{2.4}$$

The minimization (2.4) is the synthesis-based approach which assumes that the image can be synthesized from a sparse frame coefficient vector v by $u := W^T v$. It is seen that the two minimization formulations (2.3) and (2.4) will yield different results when $WW^T \neq I$. The

synthesis-based approach (2.4) emphasizes more the sparsity of the solution, as it finds the solution in a larger space than the analysis-based approach (2.3). Instead, the analysis-based approach (2.3) emphasizes the balance between the sparsity of frame coefficients and the smoothness of the solution, as the term $\|Wu\|_1$ is linked to the smoothness of the underlying function [5]. When $0 < \beta < \infty$, the minimization (2.2) is called the balanced approach, which has been used with $\beta = 1$ and $p = 2$ in image inpainting [11, 12]. For our purpose, it is empirically observed that the analysis-based approach (2.3) is likely to yield the results with more pleasant visual quality, and there also exists an efficient numerical solver as discussed in the following section.

2.2. Numerical Computation

The numerical method to solve the minimization problem (2.1) was very computationally expensive with excessive memory requirements. Recently, a so-called *split Bregman iteration* [28] proved to be efficient for solving a class of ℓ_1 related minimization problems. The Bregman iteration was first introduced to the image processing community in [36] and was then applied to a variety of signal and image processing problems. The split Bregman iteration extends the utility of the Bregman iteration to a more general class of ℓ_1-norm related minimization problems with the convergence proved in [16]. The basic idea is to convert (2.1) by introducing one more constraint involving an auxiliary variable $d = Wu$, and then invoking the Bregman iteration to solve the constrained minimization problem. The split Bregman algorithm is particularly suitable for many image restoration tasks as it converges fast, uses a small memory footprint and is easy to implement. The application of split Bregman iteration to some existing algorithms in optimization is pointed out by [26, 39]. In fact, the split Bregman algorithm is equivalent to the alternating direction method of multipliers and the Douglas-Rachford splitting algorithm for the dual problem.

We use the split Bregman iteration to solve the minimization problem (2.1). The iterative algorithm is outlined here, and more detailed discussions of the algorithm may be found in [16, 28]. Consider a general ℓ_1 minimization problem

$$\min_u \quad E(u) + \lambda \|Lu\|_1, \tag{2.5}$$

where $E(u)$ is a smooth convex function and L is a linear operator. Let $u^0 := 0, d^0 = b^0 := 0$ be the initial seeds, when the split Bregman algorithm for (2.5) is as follows:

$$\begin{cases} u^{k+1} := \arg\min_u E(u) + \frac{\mu}{2}\|Lu - d^k + b^k|_2^2, \\ d^{k+1} := \mathscr{T}_{\lambda/\mu}(Lu^{k+1} + b^k), \\ b^{k+1} := b^k + (Lu^{k+1} - d^{k+1}), \end{cases} \tag{2.6}$$

where $\mu > 0$ is a parameter of the algorithm, and T_θ is the soft-thresholding operator defined by

$$\mathscr{T}_\theta : x = [x_1, x_2, \cdots, x_M] \to \mathscr{T}_\theta(x) = [t_\theta(x_1), t_\theta(x_2), \cdots, t_\theta(x_M)],$$

where

$$t_\theta(\xi) = \text{sgn}(\xi) \max\{0, |\xi| - \theta\}.$$

During the iteration (2.6), the second and the last step are both trivial to compute. The computation of the first step varies with different choices of function $E(u)$.

For solving the minimization problem (2.1), the split Bregman iterations are described for both $p = 1$ and $p = 2$, respectively. For $p = 2$, the first step in the split Bregman iteration is to find a least squares solution. Let $E(u) = \frac{1}{2}\|P_\Lambda(Hu - f)\|_2^2$ and let $L = W$. The corresponding algorithm is

$$\begin{cases} u^{k+1} := (H^T P_\Lambda H + \mu W^T W)u = H^T P_\Lambda f + \mu W^T(d^k - b^k), \\ d^{k+1} := \mathscr{T}_{\lambda/\mu}(Wu^{k+1} + b^k), \\ b^{k+1} := b^k + (Wu^{k+1} - d^{k+1}) \end{cases} \tag{2.7}$$

with the initialization $u^0 =$ and $d^0 = b^0 = 0$. The stopping criterion adopted is $\|d^k - Wu^k\| \leq \epsilon$ with ϵ being a given tolerance. The main computational cost of the iterative scheme (2.7) lies in solving the linear system in the first step. If all pixels are available ($\Lambda = \Omega$), then the linear system can be solved efficiently in the Fourier domain by using a periodic boundary condition, since the matrices $H^T H$ and $W^T W$ are circulant and can be diagonalized by fast Fourier transform (see *e.g.* [42]). However, such an approach does not work when there is missing data, as the circulant structure is lost even using a periodic boundary extension. In our approach, the symmetric boundary extension is used as it causes less boundary artifacts in the results. The resulting linear system in (2.7) is positive definite and therefore can be solved by the conjugate gradient (CG) method. It is emphasized that a very accurate numerical solution of the linear system (2.7) is unnecessary at each split Bregman iteration, and instead an approximate solution turns out to be adequate. Thus only a few CG iterations are used to generate an approximate solution of (2.7) in our implementation.

For the case of $p = 1$, both the data fidelity term and the regularization term in (2.1) are based on the ℓ_1-norm that is not differentiable. Thus the split Bregman iteration in (2.6) should be modified accordingly. The term E vanishes but, in addition to the quadratic functional in the first step of (2.6), another quadratic functional related to the ℓ_1 norm based data fidelity term comes into the first step and the corresponding coefficient vectors are updated in a similar way as for the regularization term $\|Lu\|_1$. The corresponding split Bregman iteration for the case of $p = 1$ is

$$\begin{cases} u^{k+1} := (\mu_1 H^T P_\Lambda H + \mu_2 W^T W)u = \mu_1 H^T P_\Lambda(v^k - w^k + f) + \mu_2 W^T(d^k - b^k) \\ v^{k+1} = \mathscr{T}_{1/\mu_1}(Hu^{k+1} - f + w^k) \\ d^{k+1} = \mathscr{T}_{\lambda/\mu_2}(Wu^{k+1} + b^k) \\ w^{k+1} = w^k + (Hu^{k+1} - v^{k+1} - f) \\ b^{k+1} = b^k + (Wu^{k+1} - d^{k+1}) \end{cases} \tag{2.8}$$

where μ_1 and μ_2 are the algorithm parameters related to the data fidelity term and regularization term, respectively. The initialization is set to be $u^0 = w^0 = 0$ and $d^0 = b^0 = 0$.

Similar to (2.7), the linear system in the first step of (2.8) can be solved using the CG method, and in the implementation only an approximate solution on running a few CG iterations is used. Both iterations (2.7) and (2.8) are very efficient, as demonstrated by numerical simulations in Section 3.

3. Applications

The model considered in (2.1) is quite general, and can be applied to many image restoration tasks in the presence of missing pixels or pixels with heavily distorted intensity. In this section, we will demonstrate three such applications: 1) simultaneous image deblurring and inpainting; 2) super-resolution image reconstruction; and 3) image deblurring in the presence of impulse noise. The details of each application and its formulation as a special case of (2.1) are given in the remainder of the section, and the results are compared with some existing methods. The performance of the method is evaluated in terms of both visual quality and the PSNR value of the restored images. Recall that the peak signal to noise ratio (PSNR) is defined by

$$\text{PSNR} = 10 \log_{10} \frac{255^2}{\frac{1}{mn} \sum_{i=1}^{m} \sum_{j=1}^{n} (\widehat{x}_{ij} - x_{ij})^2},$$

where m and n are the width and height of the image, and x_{ij} and $\widehat{x}_{ij}$ are the intensity values of the original image and of the restored image, respectively.

3.1. Simultaneous Image Deblurring and Inpainting

In many situations, some regions of the image could be damaged or lost – *e.g.* there are scratches on film frames or un-wanted texts are written on the images. The goal of image inpainting is then to fill in (or interpolate) the missing or damaged pixels based on the available information of the image. The problem of image inpainting has been extensively studied since the pioneering work in [4], and reference may also be made to [20] for a thorough review on this topic. In this subsection, we address a more complicated image degradation problem – viz. images are blurred and pixels are missing in some regions. Let Λ denote the index set of available pixels. The corresponding image degradation model is then

$$f|_{\Lambda} = (Hu)|_{\Lambda} + \epsilon,$$

where f is the blurred image, u is the latent image, H is the matrix form of the convolution with some blurring kernel and ϵ is additive Gaussian white noise. Presumably, the blur kernel is known from other sources and the missing pixels are identified accurately by some pre-process or by user interactions. Then, the goal of image restoration is to recover the latent image u by simultaneously deblurring and inpainting $f|_{\Lambda}$.

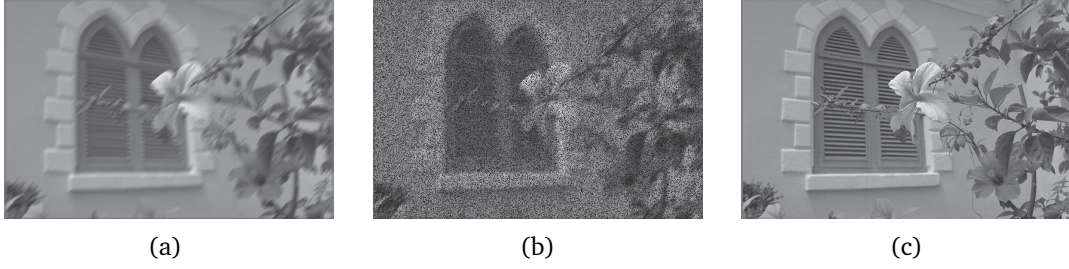| (a) | (b) | (c) |

Figure 1: Simultaneous image deblurring and inpainting. (a) Image blurred by the motion-blur kernel generated from MATLAB function $fspecial('motion', 15, 45)$, (b) blurred image with 30% randomly missing pixels, (c) the restored image with the PSNR value of 40.25dB. $\lambda = 0.001$ is used in the algorithm.

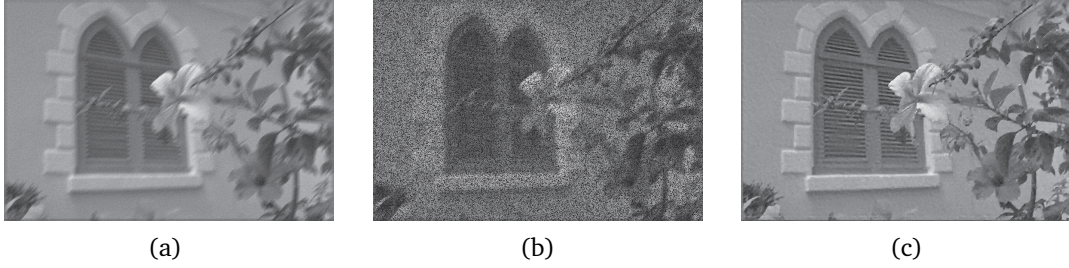| (a) | (b) | (c) |

Figure 2: Simultaneous image deblurring and inpainting. (a) Noisy blurred image, (b) noisy blurred image with 30% missing pixels, (c) restored image with the PSNR value of 27.76 dB. $\lambda = 0.3$ is used in the proposed algorithm.

The minimization based approach (2.1) is used to solve such an image restoration problem with $p = 2$ – i.e.

$$\min_{u} \quad \frac{1}{2}\|P_{\Lambda}(Hu - f)\|_2^2 + \lambda\|Wu\|_1; \tag{3.1}$$

ℓ_2 is used as the distance function of the fidelity term as the image noise is assumed to be i.i.d., and for Gaussian noise $N(0, \sigma^2)$. Two types of missing pixels are studied in the numerical experiments – viz. randomly missing pixels and non-randomly missing pixels. In the first experiment, the sample image is blurred by a linear diagonal motion blur kernel of 15-pixel length, and 30% of all pixels are randomly missing. The result from the proposed algorithm is shown in Fig. 1 in the absence of image noise. It is seen that the visual quality is nearly perfect with a high PSNR value of 40.25 dB. In the presence of image noise, the result is shown in Fig. 2 for the case of noise variance $\sigma = 5$. The visual quality of the recovered image is still quite good with a respectable PSNR value of 27.76 dB. It is noted that the appropriate value of λ is determined by the noise level of the image. In the experiments, a small value of $\lambda = 0.001$ is used when there exists no image noise, and a relative large value of $\lambda = 0.3$ when there exists noticeable image noise (with $\sigma = 5$).

In the second experiment, the missing pixels of the tested image are not random. Instead, the pixels are missing due to scratches in the films or by texts on the images, and
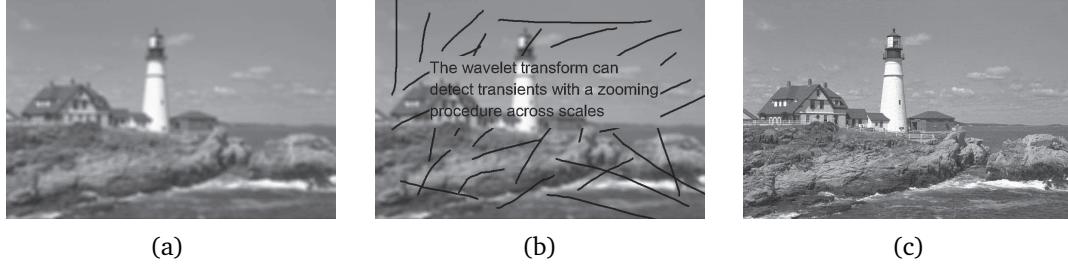
(a) (b) (c)

Figure 3: Simultaneous image deblurring and inpainting. (a) Image blurred by an out-of-focus kernel of radius 6 pixel, generated by Matlab function $fspecial('disk',6)$, (b) iblurred mage with scratches and inserted texts, (c) restored image with the PSNR value of 34.27 dB. $\lambda = 0.0005$ is used in the algorithm.
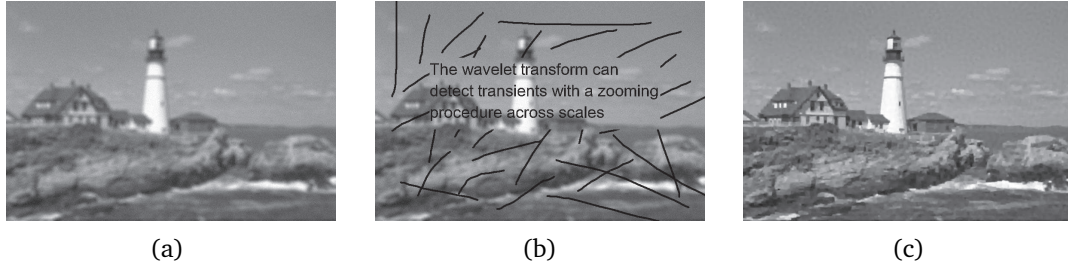

(a) (b) (c)

Figure 4: Simultaneous image deblurring and inpainting. (a) Image blurred by an out-of-focus kernel of radius 6 pixels and corrupted by additive Gaussian white noise with $\sigma = 5$, (b) image with scratches and inserted texts, (c) restored image with the PSNR of 24.43 dB. $\lambda = 0.3$ is used in the algorithm.

the image is also blurred by an out-of-focus kernel. The results shown in Fig. 3 are in the absence of image noise, and those in Fig. 4 in the presence of image noise with $\sigma = 5$. It is observed that the proposed algorithm is still quite capable of simultaneously deblurring and inpainting images with non-randomly missing pixels.

3.2. Super-resolution Image Reconstruction

Super-resolution image reconstruction from multiple sensors is one technique in the imaging industry to capture a high-resolution image from an array of low-resolution images. The array of low-resolution images are captured by an array of image sensors, with pre-arranged image displacements between the images. In this section, we adopt the model of the array of image sensors proposed by Bose and Boo [6]. Consider a $K \times K$ sensor array in which each sensor (p,q) produces an image of resolution $m \times n$, denoted by f_{pq} for $p,q = 1,2,\ldots,K$. The goal of super-resolution imaging is to reconstruct a high-resolution image of size $M \times N$ from a full (or partial) set of these low-resolution frames with $M = Km$, $N = Kn$. The relationship between each individual low-resolution frame and the underlying high-resolution image can be modeled by a blurring process followed by a uniform sub-sampling [6, 18, 19]

$$f_{pq} = P_{\Lambda_{pq}} Hu + \epsilon_{pq}, \qquad p,q = 1,2,\ldots,K,$$

where the blurring matrix H is associated with a specific blurring kernel modeled by the tensor product of the 1D filter

$$h = \left[\frac{1}{2} \underbrace{1 \ldots 1 \ldots 1}_{K-1} \frac{1}{2} \right].$$

Here $P_{\Lambda_{pq}}$ is the projection on

$$\Lambda_{pq} = \left\{ (iK+p, jK+q), \ i = 1,2,\ldots,m, \ j = 1,2,\ldots,n \right\}, \qquad p,q = 1,2,\ldots,K,$$

a uniformly distributed index subset of the high-resolution blurred image Hu.
The practical system can either use the full array or only a portion of the image sensors. Let $\widetilde{\mathscr{S}}$ denote the set of sensors used in the system – i.e.

$$\widetilde{\mathscr{S}} \subseteq \mathscr{S} = \{(p,q), \ p,q = 1,2,\ldots,K\}.$$

The following minimization is proposed to reconstruct the high-resolution image from multiple low-resolution images:

$$\min_u \ \frac{1}{2} \sum_{(p,q)\in\widetilde{\mathscr{S}}} \|P_{\Lambda_{pq}}(Hu - f)\|_2^2 + \lambda \|Wu\|_1. \tag{3.2}$$

Notice that $P_{\Lambda_{pq}} f = f_{pq}$. The proposed minimization (3.2) is also a special case of (2.1) with

$$\Lambda = \bigcup_{(p,q)\in\widetilde{\mathscr{S}}} \Lambda_{pq}.$$

The wavelet tight frame has been used before for super-resolution images from a sensor array [18, 19], where an iterative scheme is proposed by alternately soft-thresholding in the tight frame domain and projecting the result back to image domain. It is proved in [11] that such a iterative scheme actually converges to the solution of the minimization problem

$$\min_v \ \frac{1}{2}\|P_\Lambda(HW^T v - f)\|_2^2 + \frac{1}{2}\|(I - WW^T)v\|_2^2 + \lambda \|v\|_1, \tag{3.3}$$

which is the balanced approach we discussed in Section 2. The formulation (3.3) becomes the synthesis approach when the second term vanishes. Our proposed algorithm is based on the analysis-based sparsity prior. In the experiments, the results from our proposed approach are compared against those from the balanced approach [11] and also the synthesis approach, in terms of their PSNR values.

Two images are tested in the experiments for various configurations of image sensor array. The results from our proposed algorithm are shown in Fig. 5 and Fig. 6, under different configurations of a 4×4 sensor array in the absence of image noise. Fig. 7 and Fig. 8 show the results from our proposed algorithm in the presence of image noise, with the signal-to-noise ratio of noisy images being SNR $= 30$ dB. The same set of experimental data is used for testing the algorithm in [11]. A numerical comparison of PSNR values for

Table 1: Comparison of PSNR values achieved by the analysis-based approach in this paper, the balanced approach in [11] and the synthesis approach for super-resolution image reconstruction.

	Analysis approach (# of sensor arrays)				Balanced approach (# of sensor arrays)				Synthesis approach (# of sensor arrays)			
	16	8	4	1	16	8	4	1	16	8	4	1
Boat	31.3	31.1	28.2	24.9	29.8	29	26.8	23.9	30.8	29.5	27.6	22.9
Goldhill	29.2	28.5	27.2	25.4	28.5	27.9	26.5	24.6	28.9	28.1	27.0	23.5

the noisy case in Table 1 shows that our algorithm consistently outperforms the balanced approach proposed in [11], with average $1-2$ dB gain in PSNR. The gain over the synthesis approach is about $0.5 - 2$ dB. The results indicate that the analysis-based approach is more suitable for the application of super-resolution imaging than the synthesis/balanced approach.

In addition, the split Bregman iteration is extremely efficient in solving the minimization problem (3.2). It is observed in the experiment that a sufficiently accurate solution can be obtained within 10 iterations, and 30 seconds running time in MATLAB code on a desktop PC with a 2Ghz Intel CPU. In comparison, the algorithm proposed in [11] is quite slow and requires much more computational time. We note that the recent accelerated proximal gradient (APG) algorithm [3, 40] substantially accelerates the balanced approach in [11], and takes less time to obtain a satisfactory solution in the same hardware configuration. Hence, we also employ the APG algorithm for computation in the synthesis approach.

3.3. Image Deblurring in the Presence of Impulsive Noise

In this section, we consider how to recover blurred images corrupted by both additive Gaussian noise and impulsive noise. Gaussian noise caused by thermal noise is prevalent in imaging systems and impulsive noise is caused by dead pixels, analog-to-digital converter errors, bit errors in transmission, etc. (see *e.g.* [7]). Such image degradation can be modeled by

$$f = N_p(Hu + \epsilon), \tag{3.4}$$

where f and u are the observed and the latent image respectively, H is the matrix of blurring, ϵ is the Gaussian noise and N_p represents the process which affects image pixels by impulse noise. Let the dynamic range of f be $[d_{min}, d_{max}]$. There are two main types of impulsive noise – viz. salt-and-pepper noise and random valued impulsive noise, which are characterized as follows:

- *Salt-and-pepper noise,* where a certain proportion of pixels are altered to be either d_{min} or d_{max}, i.e.

$$N_p(x_{ij}) = \begin{cases} d_{min}, & \text{with probability } s/2 \\ d_{max}, & \text{with probability } s/2 \\ x_{ij}, & \text{with probability } (1-s) \end{cases}$$

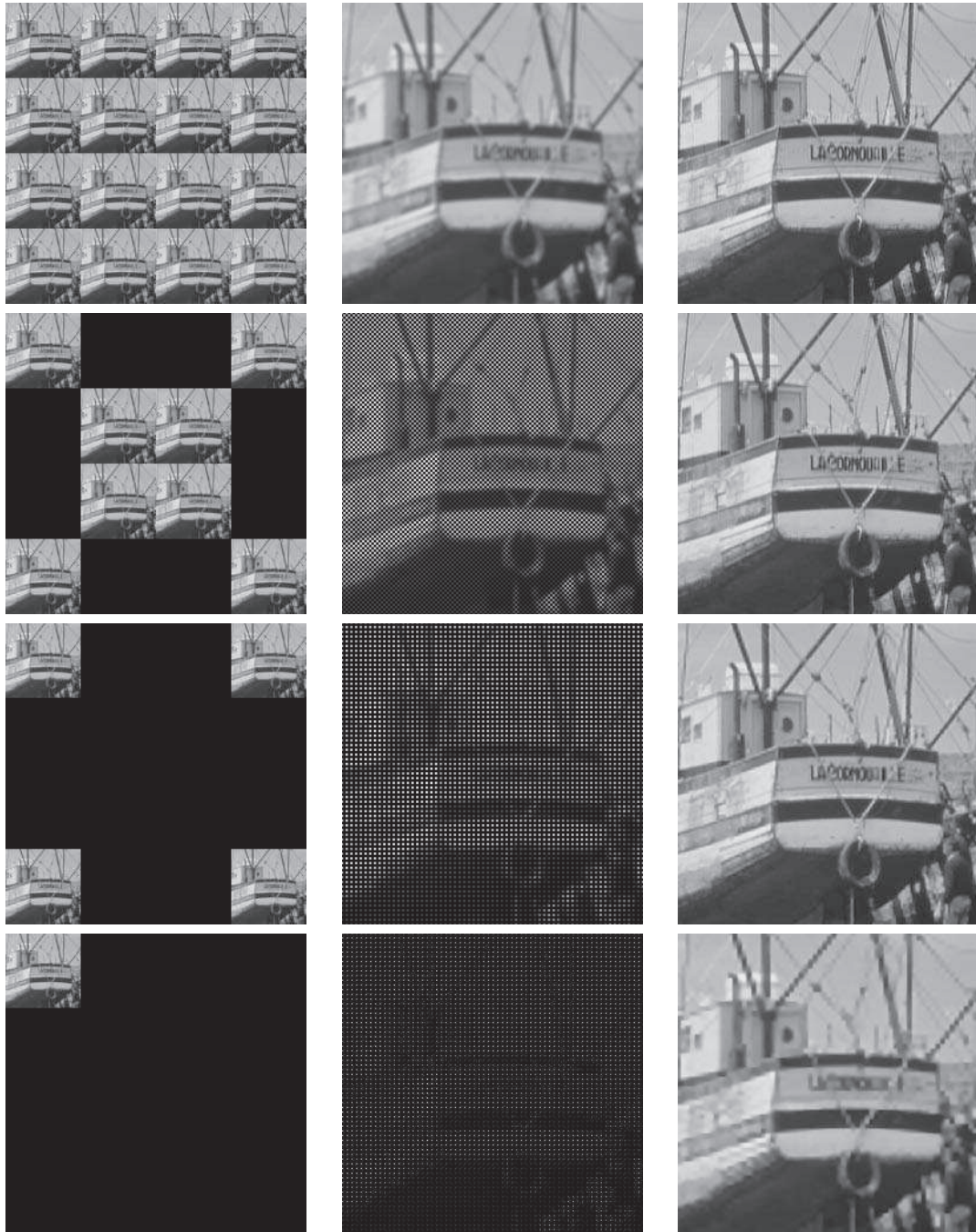where s is the level of salt-and-pepper noise.

Figure 5: Super-resolution image reconstruction on "Boat". Columns represent (from left to right) the available low-resolution images, the observed high-resolution images, the reconstructed high-resolution images. The PSNRs achieved in each reconstruction (from top to bottom) are 39.5 dB,35.1 dB, 30 dB, 25.1 dB respectively.
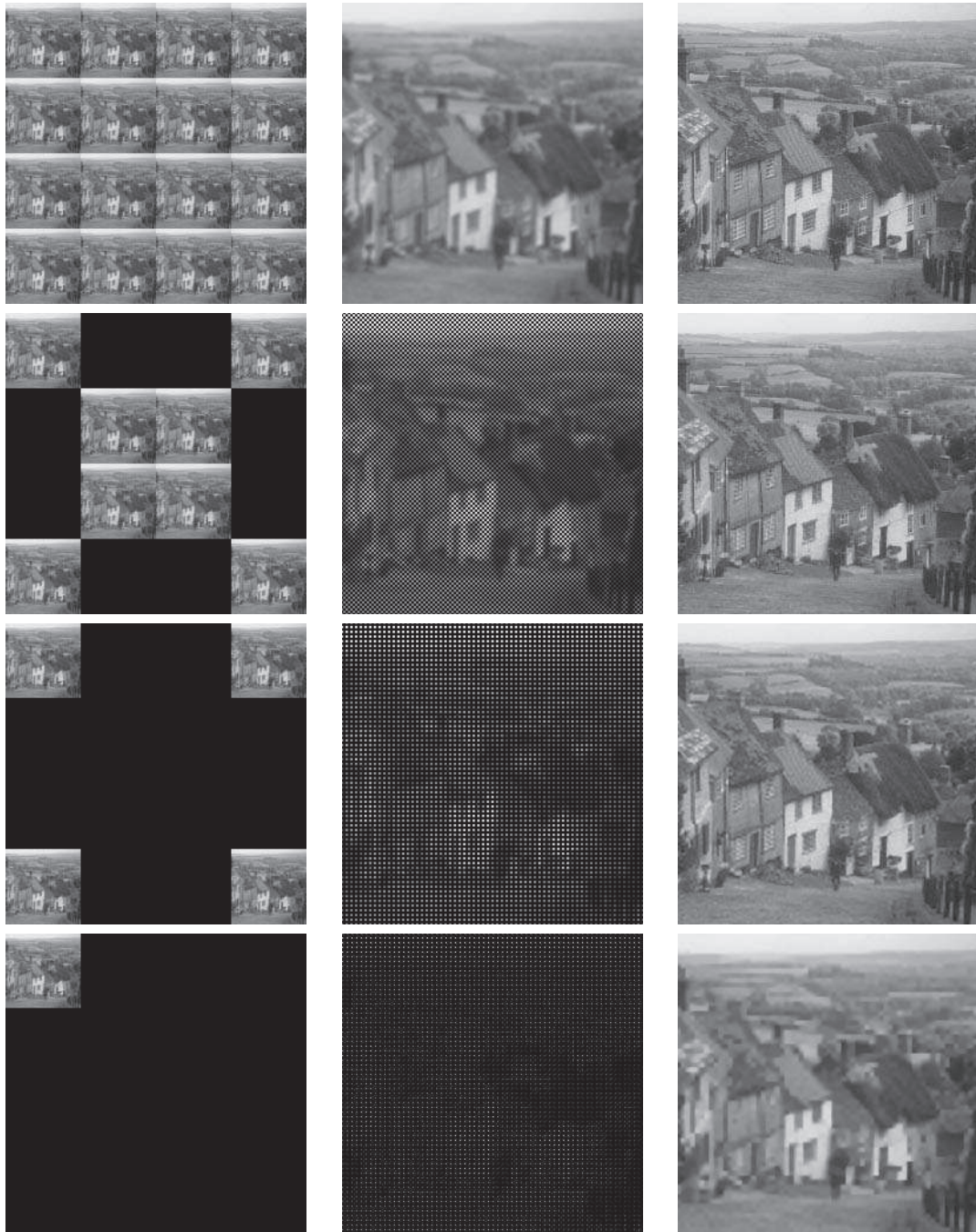
Figure 6: Super-resolution image reconstruction on "Goldhill". Columns represent (from left to right) the available low-resolution images, the observed high-resolution images, the reconstructed high-resolution images. The PSNRs achieved in each reconstruction (from top to bottom) are 37.3 dB, 31.9 dB, 28.7 dB, 25.6 dB respectively.

Figure 7: Super-resolution image reconstruction on "Boat" (SNR = 30 dB). Columns represent (from left to right) the available low-resolution images, the observed high-resolution images, the reconstructed high-resolution images. The PSNRs achieved in each reconstruction (from top to bottom)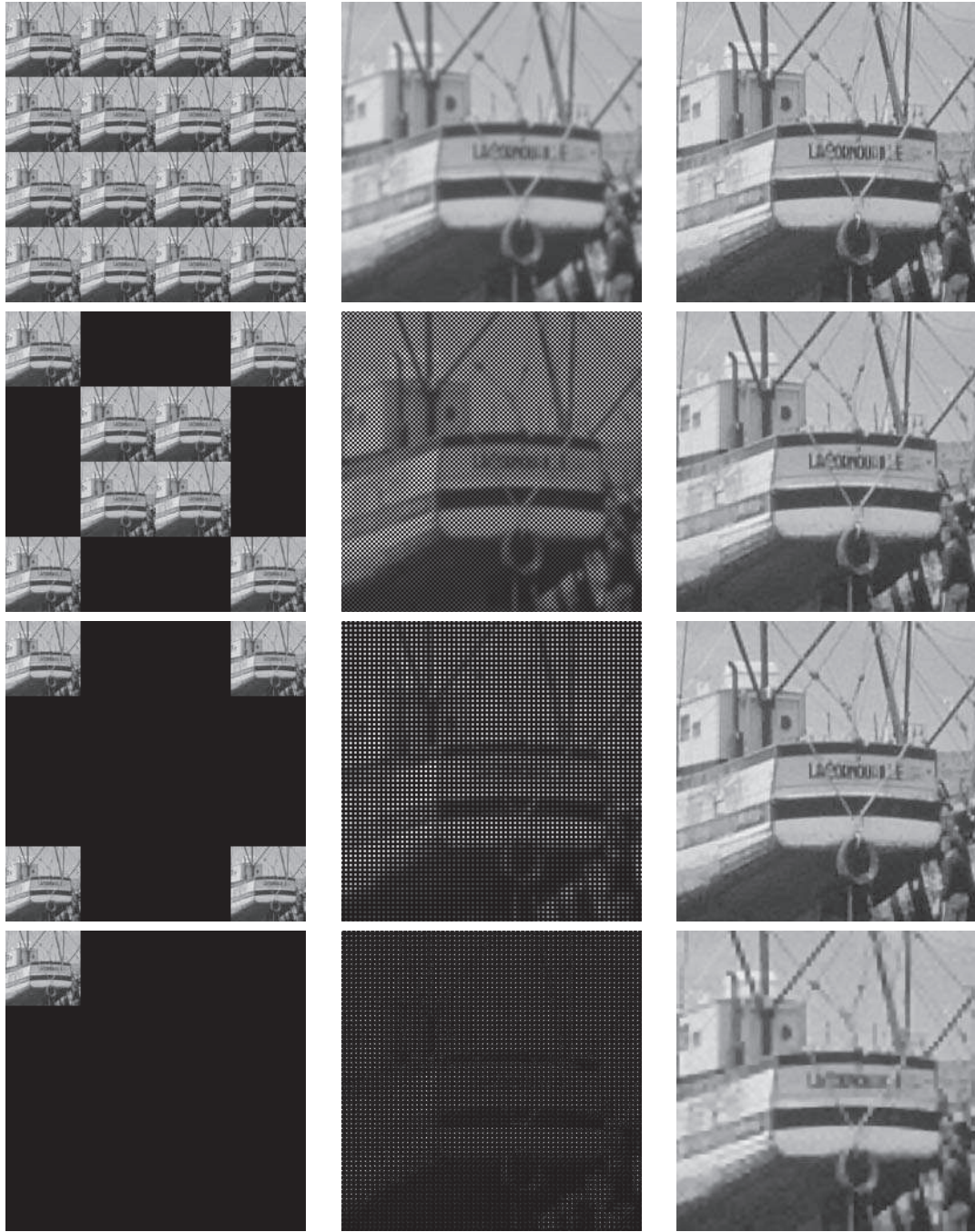 are 31.3 dB, 31.1 dB, 28.2 dB, 24.9 dB respectively. In contrast, the PSNRs achieved by the algorithm in [10] on the same set of experiments are 29.76 dB, 29.01 dB, 26.78 dB, 23.91 dB respectively.
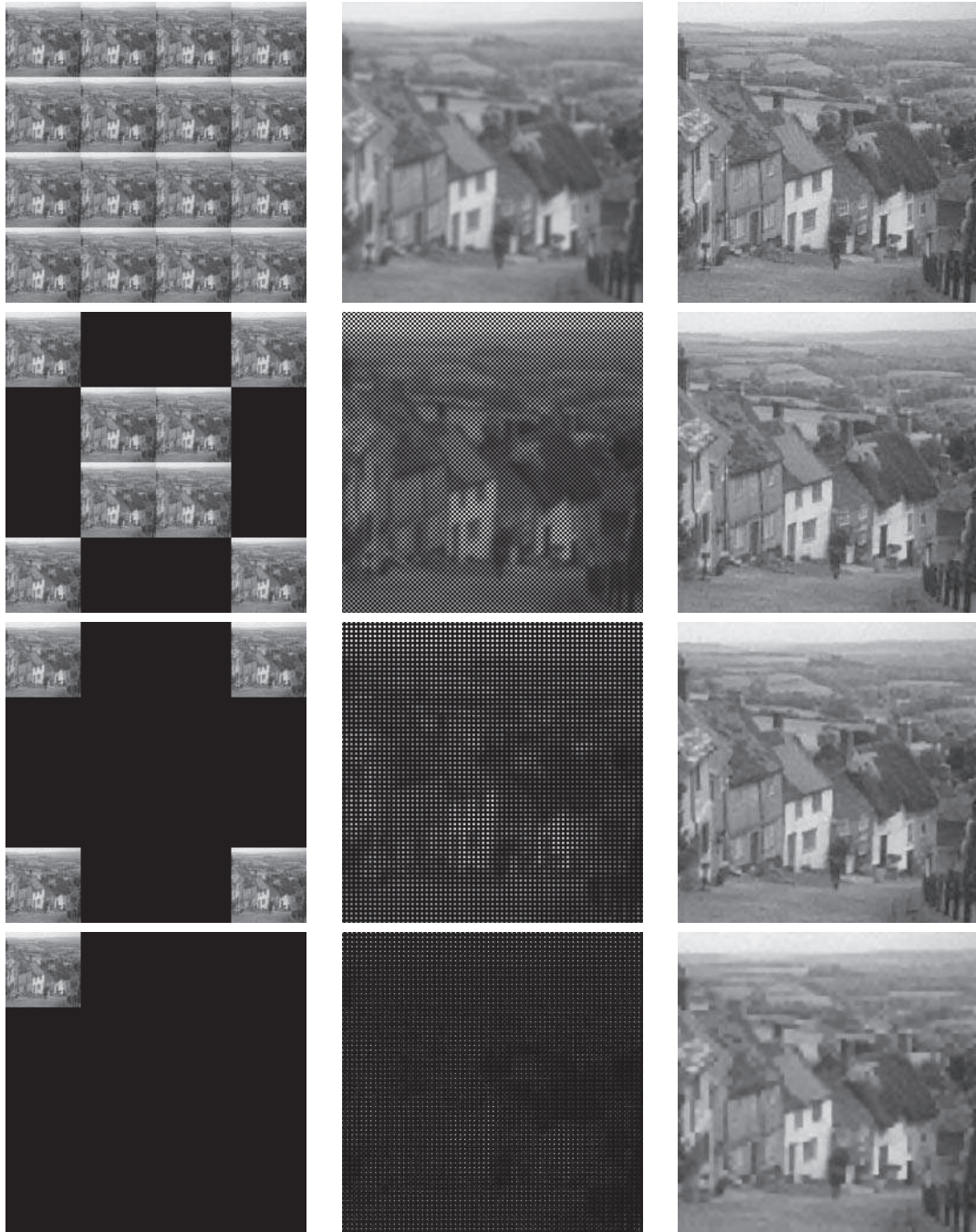
Figure 8: Super-resolution image reconstruction on "Goldhill" ($\mathrm{SNR} = 30\mathrm{dB}$). Columns represent (from left to right) the available low-resolution images, the observed high-resolution images, the reconstructed high-resolution images. The PSNRs achieved in each reconstruction (from top to bottom) are 29.20 dB, 28.46 dB, 27.24 dB, 25.42 dB. In contrast, the PSNRs achieved by the algorithm in [10] on the same set of experiments are 28.51 dB, 27.93 dB, 26.48 dB, 24.58 dB.

- *Random valued impulsive noise,* where a certain proportion of pixels are altered to be a (uniform) random number in $[d_{min},\ d_{max}]$ – viz.

$$N_p(x_{ij}) = \begin{cases} d_{ij}, & \text{with probability } r \\ x_{ij}, & \text{with probability } (1-r) \end{cases}$$

where d_{ij} is a uniformly distribution random number in $[d_{min},\ d_{max}]$ and r is the level of random valued noise.

As the content of pixels contaminated by impulsive noise contains little information of the original image content, these damaged pixels are viewed as outliers, and there has been some research [1, 2] on developing image deblurring algorithms robust to outliers. However, when images are corrupted by significant impulsive noise, there are too many outliers to be handled well by these robust methods. Recently, two-phase based approaches proposed in [8, 9] demonstrated better performance on deblurring images in the presence of impulsive noise. The basic idea of the two-phase based approach is to first detect pixels corrupted by impulsive noise and then to deblur images using only those reliable pixels. The detection of image pixels corrupted by impulsive noise has been studied extensively in the application of removing impulsive noise from images. Median filtering [21, 22, 32] is the predominant available technique for detecting pixels with impulsive noise. As the damaged pixels contain little information of the original image content, a reasonable approach is to remove them from the deblurring process by treating them as missing pixels. Let Λ denote the index set of those reliable pixels. We propose the same minimization formulation as (2.1) to deblur images:

$$\min_u \ \frac{1}{p}\|P_\Lambda(Hu - f)\|_p^p + \lambda\|Wu\|_1. \tag{3.5}$$

The main difference between our proposed approach and the two other approaches proposed in [8, 9] lies in the regularization term. The algorithm used in [8] employs the Mumford-Shah function as the regularization term and the algorithm proposed in [9] adopts a TV-like regularizer due to consideration of computational efficiency. It is noted that although (3.5) is very similar to (3.1) used in the application of simultaneous image deblurring and inpainting, the differences between them lie in the accuracy of the index set Λ. The index set Λ in (3.1) is assumed to be free of error. On the contrary, the index set Λ in (3.5) could contain wrongly detected damaged pixels or undetected damaged pixels, especially for the case of random valued impulsive noise.

The performance of the two-stage based image deblurring methods proposed in [8, 9] is dependent on the accuracy of detecting damaged pixels. We adopt the same median filter techniques used in [8, 9] to locate damaged pixels – the adaptive median filter (AMF) in [30] is used to detect salt-and-pepper noise, and the adaptive center-weighted median filter (ACWMF) in [22] is used to detect random valued impulsive noise (cf. [22, 30] for more details). It is noted that any other impulsive noise detection technique can also be used in our approach. The reason we choose these two median filter techniques is for a

fair comparison with existing methods, as the main contribution of our proposed algorithm lies in the second stage.

The detection accuracy of impulsive noise is different for the two types of impulsive noise. The detection of salt-and-pepper noise is relatively easy and is indeed very accurate with little error. On the contrary, the detection of random valued impulsive noise is much more difficult and there will be a lot of outliers in the set of detected reliable pixels. Thus, different p norms are used in these two cases:

A. If there is only salt-and-pepper noise in the image, the detection of damaged pixels using the AMF filter is very accurate and $f|_\Lambda$ is nearly free of error. In such a case, we choose $p = 1$ since that allows exact data fitting, i.e. $(Hu)_{ij} = f_{ij}$ if f_{ij} is not corrupted, while $p = 2$ cannot do this [34, 35].

B. If there is a mixture of both salt-and-pepper noise and Gaussian noise in the image, the AMF filter still can accurately locate pixels damaged by salt-and-pepper noise. Thus $f|_\Lambda$ contains only Gaussian noise. In this case, a 2-norm is used in (3.5) based on statistical maximum likelihood reasoning.

C. If the image is contaminated by random valued impulse noise, the ACWMF filter is able to identify impulse noise reasonably well, but with a noticeable amount of wrongly marked pixels. Thus, f_Λ contains a noticeable amount of outliers, when $p = 1$ is used in (3.5) for its robustness to outliers.

D. If the image is contaminated by both random-valued impulse noise and Gaussian noise, it is very difficult to detect small impulse noise as it is similar to Gaussian noise. It is suggested in [8] that either $p = 1$ or $p = 2$ can be chosen depending on the level of impulse noise and Gaussian noise, and $p = 1$ is used in our proposed approach.

In the first experiment, both the full variational approach ($\Lambda = \Omega$ in (3.5)) and the two-phase based approach are applied to illustrate the advantages of the two-phase based approach. In the experiments, the tested images are blurred by the out-of-focus blurring kernel of radius 3 pixels and then corrupted by different levels of salt-and-pepper noise. The results are shown in Fig. 9. It is seen that the performance of two approaches is close in the case of a low noise level such as 10%. However, the performance of the full variational approach is significantly degraded with the increase of the noise level. Indeed, the two-stage based approach is much more consistent and performs quite well even for the case of a noise level high as 70%. This experiment clearly indicated the advantage of the two-stage based approach over the full variational approach.

In the second experiment, our proposed two-stage algorithm is compared against two existing two-phase algorithms developed in [8, 9], on different images contaminated by different configurations of image noise. The same experimental settings are used in the comparison. The first data set involves various images with out-of-focus blur of radius 3 pixels and then corrupted by different levels of salt-and-pepper noise. The results on tested images at the noise level $s = 70\%$ are shown in Fig. 10. The PSNR values of the results from our algorithm under different noise level are given in Table 2 and compared against that from the two methods in [8, 9]. It is seen from Table 2 that our results achieved
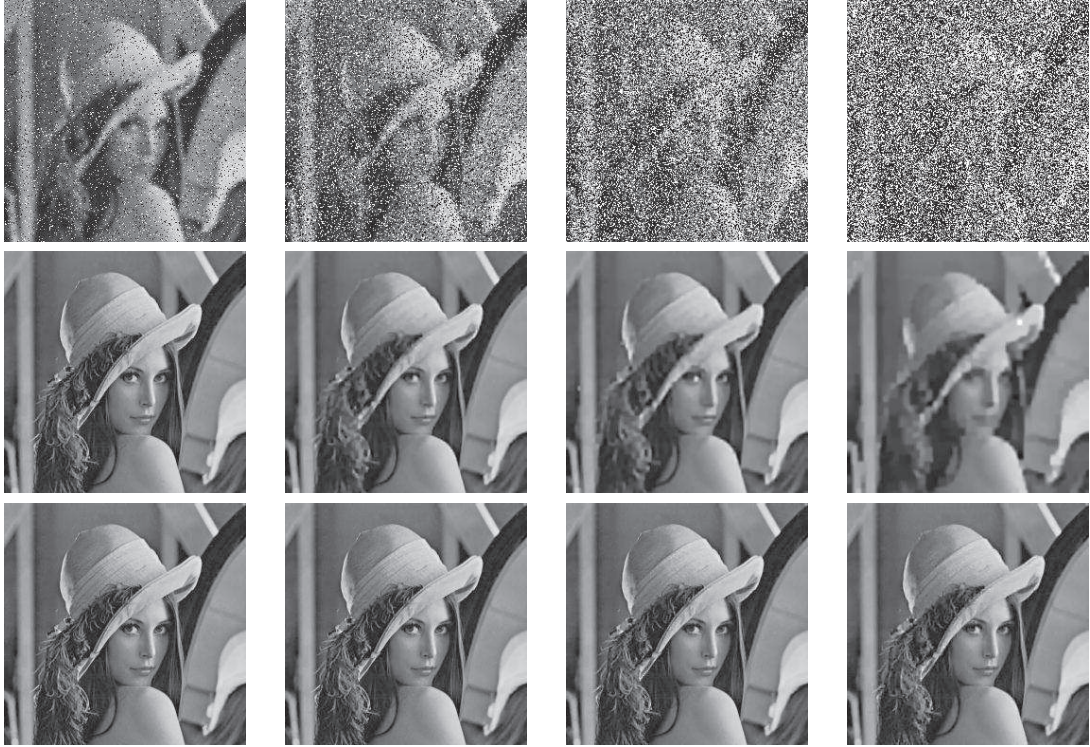
Figure 9: The top row (from left to right) shows the images to be restored, which are blurred by out-of-focus kernel of radius 3 pixels and corrupted consecutively by $10\%, 30\%, 50\%, 70\%$ salt-and-pepper noise. The middle row shows the restored images by the full variational algorithm; the corresponding PSNR values are $36.09, 29.84, 27.58, 24.13$ respectively. The bottom row shows the restorations by the two-phase algorithm; the corresponding PSNR values are $42.51, 38.60, 35.08, 31.65$ respectively.

higher PSNR values, with about $2 - 3$ dB gain over the one in [8] and about 1dB gain over the one in [9] when the noise level is lower than 50%. The advantage of our proposed algorithm is not so much when the noise level is high, as the available reliable pixels are not enough to constrain the image well. It is noted that the computational time needed in our algorithm is much less than that reported in [8,9]. Such computational efficiency is mainly from the adoption of the split Bregman algorithm. Our proposed algorithm converges fast and the results are visually indistinguishable after a few iterations (20 iterations in this experiment).

The second data set includes images corrupted by different levels of random-valued impulse noise. Random-valued impulse noise is much more difficult to detect than salt-and-pepper noise. The ACWMF filter is used to detect random-valued impulsive noise in the first phase of our proposed algorithm. There are unavoidably outliers in the detected reliable pixels and thus the ℓ_1-norm is used as the distance function in the fidelity term of (3.5). The ℓ_2-norm is not a good choice in the presence of outliers, as it is shown in [31] that the results can be either over-smoothed by using a large regularization parameter or attracted to the outliers by using a small regularization parameter. The advantage of using

Table 2: Comparison of PSNR and computational time (seconds) between our algorithm and two other algorithms [8, 9] in the presence of salt-and-pepper noise. The blurring kernel is the out-of-focus of radius 3 pixel.

Image	Ratio	Our algorithm		Algorithm in [9]		Algorithm in [8]	
		PSNR	Time	PSNR	Time	PSNR	Time
Lena	30%	38.6	42	37.5	187	35.9	504
	50%	35.0	42	33.7	212	32.7	496
	70%	31.7	39	30.7	239	30.1	488
	90%	27.3	32	27.1	335	26.7	623
bridge	70%	27.2	42	26.4	241	26.2	514
baboon	70%	25.2	42	24.7	223	24.7	452
boat	70%	28.7	42	27.7	231	26.7	488
goldhill	70%	29.5	41	28.8	208	28.4	402

Figure 10: Restoration results for the corrupted images with the out-of-focus kernel of radius 3 and 70% salt-and-pepper noise. The PSNR values of the results are given in Table 2.

Figure 11: From left to right shows the corrupted image with the out-of-focus kernel of radius 3 pixels and 40% random-valued impulse noise, the intermediate output from median filtering, the restoration by using ℓ_2-norm based data fidelity term in (3.5) and the restoration by using ℓ_1-norm based data fidelity term in (3.5).

the ℓ_1 norm over the ℓ_2 norm in the presence of outliers is clearly demonstrated in Fig. 11. The PSNR values of the results from our algorithm are listed in Table 3 for different levels of impulsive noise, and compared against those in [8, 9]. Overall, about $1 - 2$ dB gain of the PSNR value over that from [8, 9] is achieved by our algorithm when the noise level is less than 60%. The advantage of our proposed algorithm over those in [8, 9] is much less noticeable in the presence of high-level random-valued impulse noise.

Lastly, we come to the case when both Gaussian noise and impulse noise are present

Table 3: Comparison of PSNR and computational time (seconds) between our algorithm and two other algorithms [8,9] under random-valued impulse noise. The blurring kernel is the out-of-focus of radius 3.

Image	Ratio	Our algorithm		Algorithm in [9]		Algorithm in [8]	
		PSNR	Time	PSNR	Time	PSNR	Time
Lena	10%	40.2	46	35.6	65	38.7	584
	25%	36.3	49	32.8	66	34.4	606
	40%	32.4	63	30.5	68	31.2	739
	55%	28.6	70	27.2	104	27.8	784
bridge	40%	27.8	63	26.4	81	27.3	726
baboon	40%	25.7	56	24.7	64	25.3	635
boat	40%	29.4	63	27.7	91	28.2	709
goldhill	40%	30.2	57	28.8	64	29.5	705

Table 4: Comparison of the PSNR value of the results from our algorithm and that from the algorithm in [8] in the presence of both Gaussian and impulse noise.

Image	Ratio	Our algorithm PSNR	Algorithm in [8] PSNR
Lena	s= 30%	27.5	27.2
	s = 50%	27.2	26.9
	s = 70%	26.7	26.4
	s = 90%	25.2	24.7
	r = 10%	27.3	27.2
	r = 25%	27.1	27.0
	r = 40%	26.8	26.7

in the blurred image. The tested images are "lena" blurred by out-of-focus kernel of radius 3 and then corrupted with Gaussian noise ($\sigma = 5$, SNR = 26.9 dB) followed by $30\%, 50\%, 70\%, 90\%$ salt-and-pepper noise. The PSNR of the restored images by our algorithm is given in Table 4, in which as a comparison the PSNR's achieved by the method in [8] for the same experimental setting is provided. When Gaussian noise and random-valued impulse noise are present, the corresponding figures are also as shown in Table 4. In both cases, our algorithm only achieves slight improvement over [8].

4. Brief Discussion and Possible Future Work

In this paper, we present a unified approach to recover degraded images with missing or damaged pixels for several typical image degradations. Under the analysis-based sparsity prior of images under a wavelet tight frame domain, the proposed regularization-based approach can effectively recover degraded images in the presence of missing or damaged pixels. Furthermore, the proposed approach is robust to the detection error of missing or damaged pixels, which makes it more appealing in practice. The resulting minimization can be solved efficiently by an adaptive version of the split Bregman iteration algorithm.

In our experiments on various types of image restoration tasks, our algorithm compares favorably against many existing methods. In future, we are interested in developing image restoration methods that are robust to a wide range of image noise – *e.g.* Gaussian noise, Poisson noise, impulsive noise, or a combination of these.

References

[1] Leah Bar, Nahum Kiryati, and Nir Sochen. Image deblurring in the presence of impulse noise. *Int. J. Computer Vision*, 70(3):279–298, 2006.

[2] Leah Bar, Nir Sochen, and Nahum Kiryati. Image deblurring in the presence of salt-and-pepper noise. In *Lecture Notes in Computer Science, Scale Space and PDE Methods in Computer Vision, LNCS)*, volume 3459, pages 107–118, 2005.

[3] A. Beck and M. Teboulle. A fast iterative shrinkage-thresholding algorithm for linear inverse problems. *SIAM J. Imaging Sci.*, 2(1):183–202, 2009.

[4] Marcelo Bertalmio, Guillermo Sapiro, Coloma Ballester, and Vicent Caselles. Image inpainting. In *Computer Graphics, SIGGRAPH 2000*, pages 417–424, 2000.

[5] Lasse Borup, Rémi Gribonval, and Morten Nielsen. Bi-framelet systems with few vanishing moments characterize Besov spaces. *Appl. Comput. Harmon. Anal.*, 17(1):3–28, 2004.

[6] N.K. Bose and K.J. Boo. High-resolution image reconstruction with multisensors. *J. Imaging Syst. Technol.*, 9(4):294–304, 1998.

[7] Alan C. Bovik. *Handbook of Image and Video Processing*. Academic Press Inc., San Diego, CA, 2000.

[8] Jian-Feng Cai, Raymond H. Chan, and Mila Nikolova. Two-phase approach for deblurring images corrupted by impulse plus Gaussian noise. *Inverse Probl. Imaging*, 2(2):187–204, 2008.

[9] Jian-Feng Cai, Raymond H. Chan, and Mila Nikolova. Fast two-phase image deblurring under impulse noises. *J. Math. Imaging Vis.*, 36(1):46–53, 2010.

[10] Jian-Feng Cai, Raymond H. Chan, Lixin Shen, and Zuowei Shen. Restoration of chopped and nodded images by framelets. *SIAM J. Sci. Comput.*, 30(3):1205–1227, 2008.

[11] Jian-Feng Cai, Raymond H. Chan, Lixin Shen, and Zuowei Shen. Simultaneously inpainting in image and transformed domains. *Numer. Math.*, 112(4):509–533, 2009.

[12] Jian-Feng Cai, Raymond H. Chan, and Zuowei Shen. A framelet-based image inpainting algorithm. *Appl. Comput. Harmon. Anal.*, 24(2):131–149, 2008.

[13] Jian-Feng Cai, Hui Ji, Chaoqiang Liu, and Zuowei Shen. Blind motion deblurring from a single image using sparse approximation. In *IEEE Conference on Computer Vision and Pattern Recognition*, Miami, 2009.

[14] Jian-Feng Cai, Hui Ji, Chaoqiang Liu, and Zuowei Shen. Blind motion deblurring using multiple images. *J. Comput. Phys.*, 228(14):5057–5071, 2009.

[15] Jian-Feng Cai, Stanley Osher, and Zuowei Shen. Linearized Bregman iterations for frame-based image deblurring. *SIAM J. Imaging Sci.*, 2(1):226–252, 2009.

[16] Jian-Feng Cai, Stanley Osher, and Zuowei Shen. Split bregman methods and frame based image restoration. *Multiscale Model. Simul.*, 8(14):5057–5071, 2009.

[17] Anwei Chai and Zuowei Shen. Deconvolution: a wavelet frame approach. *Numer. Math.*, 106(4):529–587, 2007.

[18] Raymond H. Chan, Tony F. Chan, Lixin Shen, and Zuowei Shen. Wavelet algorithms for high-resolution image reconstruction. *SIAM J. Sci. Comput.*, 24(4):1408–1432, 2003.

[19] Raymond H. Chan, Sherman D. Riemenschneider, Lixin Shen, and Zuowei Shen. Tight frame: an efficient way for high-resolution image reconstruction. *Appl. Comput. Harmon. Anal.*, 17(1):91–115, 2004.

[20] Tony F. Chan and Jianhong Shen. *Image processing and analysis: Variational, PDE, wavelet, and stochastic methods*. Society for Industrial and Applied Mathematics (SIAM), Philadelphia, PA, 2005.

[21] Tao Chen, Kai-Kuang Ma, and Li-Hui Chen. Tri-state median filter for image denoising. *IEEE Trans. Image Processing*, 8(12):1834–1838, 1999.

[22] Tao Chen and Hong Ren Wu. Adaptive impulse dectection using center-weighted median filters. *IEEE Signal Processing Letters*, 8(1):1–3, 2001.

[23] A. Criminisi, P. Perez, and K. Toyama. Region filling and object removal by exemplar-based image inpainting. *IEEE Trans. Image Processing*, 13(9):1200–1212, 2004.

[24] Ingrid Daubechies. *Ten lectures on wavelets*. Society for Industrial and Applied Mathematics (SIAM), Philadelphia, PA, 1992.

[25] Ingrid Daubechies, Bin Han, Amos Ron, and Zuowei Shen. Framelets: MRA-based constructions of wavelet frames. *Appl. Comput. Harmon. Anal.*, 14(1):1–46, 2003.

[26] Ernie Esser. Applications of lagrangian-based alternating direction methods and connections to split Bregman. Technical report, CAM report, UCLA, 2009.

[27] Tom Goldstein, Xavier Bresson, and Stanley Osher. Geometric applications of the split bregman method: Segmentation and surface reconstruction. Technical report, CAM report, UCLA, 2009.

[28] Tom Goldstein and Stanley Osher. The split Bregman method for $L1$-regularized problems. *SIAM J. Imaging Sci.*, 2(2):323–343, 2009.

[29] Bin Han and Zuowei Shen. Dual wavelet frames and Riesz bases in Sobolev spaces. *Constr. Approx.*, 29(3):369–406, 2009.

[30] H. Hwang and R.A. Haddad. Adaptive median filters: new algorithms and results. *IEEE Trans. Image Processing*, 4(4):499–502, 1995.

[31] Hui Ji, Zuowei Shen, and Yuhong Xu. Wavelet frame based scene reconstruction from range data. *J. Comput. Phys.* 229(6):2093–2108, 2010.

[32] S.-J. Ko and Y.H. Lee. Center weighted median filters and their applications to image enhancement. *IEEE Trans. Circuits and Systems*, 38(9):984–993, 1991.

[33] David Mumford and Jayant Shah. Optimal approximations by piecewise smooth functions and associated variational problems. *Comm. Pure Appl. Math.*, 42(5):577–685, 1989.

[34] Mila Nikolova. Minimizers of cost-functions involving nonsmooth data-fidelity terms. Application to the processing of outliers. *SIAM J. Numer. Anal.*, 40(3):965–994 (electronic), 2002.

[35] Mila Nikolova. A variational approach to remove outliers and impulse noise. *J. Math. Imaging Vis.*, 20:99–120, 2004.

[36] Stanley Osher, Martin Burger, Donald Goldfarb, Jinjun Xu, and Wotao Yin. An iterative regularization method for total variation-based image restoration. *SIAM Multiscale Model. Simul.*, 4:460–489, 2005.

[37] Amos Ron and Zuowei Shen. Affine systems in $L_2(\mathbb{R}^d)$: the analysis of the analysis operator. *J. Funct. Anal.*, 148(2):408–447, 1997.

[38] Leonid Rudin, Stanley Osher, and Emad Fatemi. Nonlinear total variation based noise removal algorithms. *Physica D*, 60:259–268, 1992.

[39] Simon Setzer. Split bregman algorithm, douglas-rachford splitting and frame shrinkage. In *Proceedings of the Second International Conference on Scale Space Methods and Variational Methods in Computer Vision 2009*, 2009.

[40] Zuowei Shen, Kim-Chuan Toh, and Sangwoon Yun. An accelerated proximal gradient algorithm for image restoration. preprint, 2009.

[41] AN Tikhonov and VA Arsenin. *Solution of Ill-posed Problems*. Winston & Sons, Washington, 1977.

[42] Junfeng Yang, Yin Zhang, and Wotao Yin. An efficient TVL1 algorithm for deblurring multi-channel images corrupted by impulsive noise. *SIAM J. Sci. Comput.*, 31(4):2842–2865, 2009.